JACS
JOURNAL OF THE AMERICAN CHEMICAL SOCIETY
Article
pubs.acs.org/JACS

Accessing Three-Dimensional Crystals with Incorporated Guests through Metal-Directed Coiled-Coil Peptide Assembly

Manish Nepal, Michael J. Sheedlo, Chittaranjan Das, and Jean Chmielewski*

Department of Chemistry, Purdue University, 560 Oval Drive, West Lafayette, Indiana 47907, United States

Supporting Information

ABSTRACT: Obtaining three-dimensional (3D) protein and peptide crystals on demand requires a precisely orchestrated hierarchical assembly of biopolymer building blocks. In this work, we disclose a metal-ion-mediated strategy to assemble trimeric coiled-coil peptides in a head-to-tail fashion into linear strands with interstrand interactions. This design led to hexagonal 3D peptide crystal formation within 30 min in the presence of divalent metal ions. The crystal morphology could be controlled by varying the metal ion/peptide ratio, resulting in hexagonal discs to rods. Diffraction studies elucidated the head-to-tail arrangement of the coiled-coil linear strands and their hexagonal, antiparallel packing within the crystal. Unsatisfied ligands at the hexagonal ends of the crystals were harnessed as a powerful means to direct His-tagged fluorophores to distinct locations within the crystals. Overall, the designed hierarchical assembly provides a facile means to obtain 3D peptide crystals and incorporate His-tag-based cargoes and may have potential use in drug delivery and sensor design.

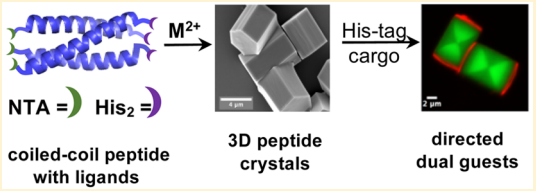

INTRODUCTION

Protein crystallization results from an impeccable assembly of protein units to form ordered structures. Crystallized proteins form the basis for structure elucidation of biological systems, and accessing these crystals is a key step in diffraction-based experiments. Protein crystals also have established roles as delivery vehicles for biopharmaceuticals and as materials for chemical catalysis.[1−4] Despite their importance, obtaining robust diffraction-quality protein and peptide crystals often entails extensive optimization. Bottom-up approaches that facilitate the formation of quality three-dimensional (3D) crystals, therefore, are highly desired.

De novo efforts to develop 3D crystalline protein and peptide materials are limited, but some notable successes have been reported.[5−10] In the seminal study of Tezcan and co-workers, strategic placement of metal-binding motifs within cytochrome *cb* 562 allowed for the formation of 2D and 3D crystalline arrays in a Zn(II)-dependent manner.[7] The 3D crystals of ferritin have also been obtained through the design of a metal/linker-directed assembly strategy.[10] In an alternate approach by Jiang and co-workers, a crystalline framework of the lectin ConA was promoted through ligand-assisted noncovalent interactions.[9] Examples of designed peptide 3D crystals are more sparse. De novo designed coiled-coil peptides of Degrado and co-workers, with engineered interactions between the coiled coils, were found to assemble into layered 3D crystals.[5,6]

Coiled-coil peptides have also been designed that undergo higher-order assembly to generate a wide range of structures, including films, fibrils and fibers, nanotubes, cages, tetrahedra, and hydrogels.[11−26] This supramolecular assembly has been achieved using hydrophobic, ionic, and hydrogen-bonding interactions. Metal ion binding has also proven to be a highly versatile means of generating self-assembled structures from peptides and proteins that is both precise and highly modular.[10,27−43] For instance, the inclusion of metal-binding ligands specifically into synthetic coiled-coil peptides for hierarchical assembly has been investigated in a limited way to produce nanospheres, nanofibers, and fibrils.[31,32,44]

In this work, we describe the programmed head-to-tail assembly of a trimeric coiled-coil peptide mediated by metal ions. This hierarchical peptide assembly has provided micron-scale 3D crystals and nano- to microspheres depending on the metal ion. A notable feature of the head-to-tail crystallization process is the availability of metal−ligand interactions at the ends of the growing crystal, a feature that has been harnessed to direct His-tagged fluorophores to specific locations within the 3D peptide crystals.

RESULTS AND DISCUSSION

Designed Hierarchical Assembly of Coiled-Coil Units.

The coiled-coil helical peptide, GCN4-p2, reported in the pioneering work by Kim and co-workers, formed the basis of our design (Figure 1a).[45] This trimeric variant of the well-studied GCN4 peptide has isoleucine residues at positions a and d in the heptad repeat to mediate the hydrophobic interactions within the parallel coiled coil. Head-to-tail assembly of these trimeric units was envisioned through metal-mediated interactions between N-terminal nitrilotriacetic acid (NTA) moieties and C-terminally displayed His residues of an adjacent coiled coil to generate GCN4-p2L (Figure 1b).

Received: June 29, 2016
Published: August 8, 2016

DOI: 10.1021/jacs.6b06708
J. Am. Chem. Soc. 2016, 138, 11051−11057

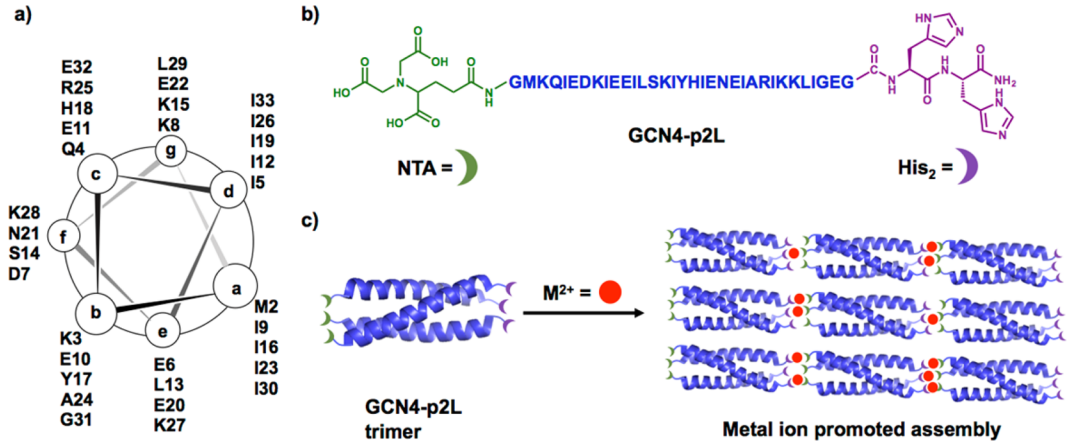

Figure 1. Design of metal-ion-mediated coiled-coil peptide assembly. (a) Helical wheel representation of the GCN4-p2 peptide, (b) sequence of the GCN4-p2L peptide with metal-binding ligands, and (c) schematic representation of the metal-triggered head-to-tail assembly of the GCN4-p2L trimeric coiled coil into linear strands, with additional interstrand electrostatic interactions mediating an antiparallel framework of the strands.

The anionic NTA ligand was placed at the N-terminus to maximize interactions with the positive end of the helical dipole, and the positively charged His residues were correspondingly placed at the C-terminal negative end of the helical dipole.[46,47] A Gly residue was placed between the ligands and each end of the GCN4-p2L peptide to provide some flexibility for metal ion binding. Metal-mediated directional assembly should promote the formation of linear stacks of trimeric coiled coils (Figure 1c). We postulated that surface-exposed residues in the coiled coils may promote further interactions. For instance, there is a clustering of positive residues at the C-termini and negative residues at the N-termini of the coiled coils. As such, we hypothesized that the linear stacks of coiled coils would favor an antiparallel packing arrangement to maximize the electrostatic interactions between the surface-exposed regions of the chains. The trimeric nature of each coiled coil would allow for radial interactions with three coiled-coil neighbors, and so on, to form an extended framework that would not be available with a dimeric coiled coil.

Synthesis and Conformation Studies. The peptide GCN4-p2L was synthesized using Fmoc-based solid phase chemistry on the ChemMatrix resin with *O*-(benzotriazol-1-yl)-*N*,*N*,*N*′,*N*′-tetramethyluronium hexafluorophosphate (HBTU) coupling. The *t*-butyl-protected NTA[48] was coupled to the N-terminus through an amide linkage with HBTU. Simultaneous cleavage from the resin and removal of side chain protecting groups was accomplished using a TFA cocktail. The peptide was purified to homogeneity using reverse-phase (RP) high-performance liquid chromatography (HPLC) and characterized by matrix-assisted laser desorption ionization time-of-flight (MALDI-TOF) mass spectroscopy. Circular dichroism (CD) was performed to determine if the modifications at the termini of GCN4-p2L perturbed the helical structure of the peptide and its ability to form a coiled coil. Minima were observed in the CD spectrum at 208 and 222 nm with a maximum peak at 193 nm as was observed with the parent GCN4-p2 peptide (Supporting Information, Figure S2).[49,50] The helical content of the GCN4-p2L was found to be 77%, a value which demonstrates that the peptide is still highly helical with the added ligands at the termini but is somewhat less helical than the parent GCN4-p2 (91%).[43] The ratio of the molar ellipticities at 222 and 208 nm was found to be 1.15, thereby confirming the coiled-coil conformation; values of approximately 1 have been demonstrated for peptides that adopt coiled-coil structures.[51]

Metal-Directed Assembly. The effect of different transition metal ions on buffered solutions of GCN4-p2L (1 mM in 20 mM 3-(*N*-morpholino)propanesulfonic acid (MOPS) buffer at pH 7.1) was evaluated. Significant turbidity was observed immediately within the solutions following the addition of metal ions such as Zn(II), Co(II), Ni(II), and Cu(II) (0.4 mM). After 30 min, the precipitates formed were collected by centrifugation, washed with water (three times), and imaged by scanning electron microscopy (SEM) (Figure 2). In the presence of Zn(II), for instance, the GCN4-p2L peptide formed 3D assemblies with a hexagonal prism morphology and dimensions of ∼4 μm in width and length (Figure 2a). Visualization of these structures under a polarizing microscope confirmed the crystalline nature of the hexagonal

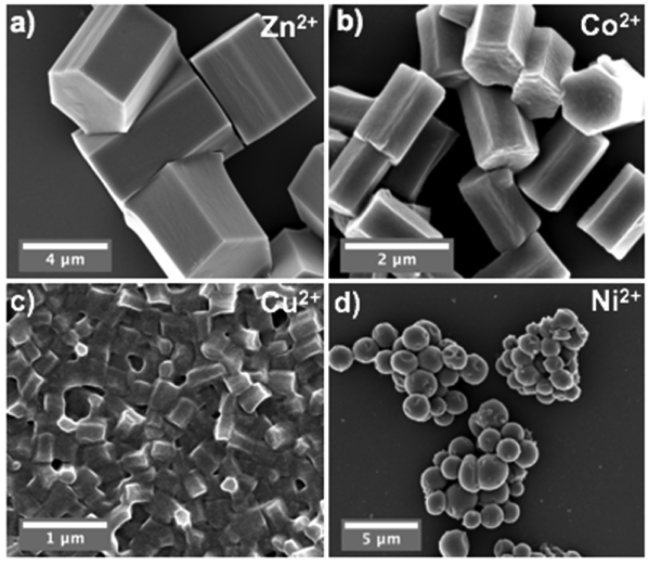

Figure 2. Higher-order assemblies formed with the GCN4-p2L peptide upon addition of divalent metal ions after 30 min. SEM micrographs of structures obtained from the assembly of GCN-p2L (1 mM) with (a) $ZnCl_2$, (b) $CoCl_2$, (c) $CuCl_2$, and (d) $NiCl_2$ (0.4 mM of each metal ion) in 20 mM MOPS buffer at pH 7.1.

DOI: 10.1021/jacs.6b06708
J. Am. Chem. Soc. 2016, 138, 11051−11057

prisms (vide infra). Structures with a similar morphology were also observed with Co(II) (Figure 2b); however, the crystals formed were slightly smaller with lengths in the 2−3 μm range and widths of ∼1 μm. Significantly smaller nanoscale hexagonal prisms were observed with Cu(II), with dimensions of ∼500 nm in length and ∼300 nm in width, which formed a densely packed network of nanoprisms (Figure 2c). Surprisingly, structures with a completely distinct morphology were observed with Ni(II) ions. Assembly of GCN4-p2L with Ni(II) resulted in interconnected spheres with diameters in the range of 0.8−2 μm (Figure 2d). It is interesting that, although the coordination geometry is different around the divalent ions of Zn, Co, and Cu, each of the peptide assemblies adopts a similar hexagonal crystalline morphology. Also, although Cu(II) and Ni(II) share a square planar coordination geometry, the structures obtained with GCN4-p2L are quite distinct. However, the binding of His to a Ni(II)−NTA complex is known to be about an order of magnitude tighter than for the corresponding Zn(II) complex,[52] and ligand exchange is slower for Ni(II) than for Zn(II).[53] With the latter in mind, a time course for the metal-directed assembly of GCN4-p2L was pursued.

Time Course of Metal-Directed Assembly. Due to the differences in metal ion/ligand exchange described above, a time course for the metal-directed assembly of GCN4-p2L was investigated with Zn(II), Cu(II), and Ni(II). Since GCN4-p2L formed well-defined hexagonal crystals within 30 min with Zn(II), we investigated the structures formed at earlier time points (5 and 15 min) to determine if there were intermediates along the path to these structures. At the shortest time point (5 min), spheres and partially formed hexagonal crystals were observed (Figure 3a), whereas after 15 min, the assemblies had almost all converted into hexagonal crystals with some nanospheres and amorphous background material present, as well (Figure 3b). Finally, at the end of 30 min, hexagonal crystals with well-defined faces and edges were observed (Figure 3c). The nanoscale interconnected hexagonal prisms obtained with GCN4-p2L and Cu(II) also completely evolved with time into micron-sized hexagonal crystals with an average length of 2.3 μm after 2 h (Figure 3d−f). Interestingly, for Ni(II) ions, the presence of nano- to micron-sized spheres was still dominant after 1 h. However, at 2 h, the spheres were now accompanied by hexagonal prisms, and after 48 h, micron-sized spheres of intertwined hexagonal rods were observed (Figure 3i). The length of the observed rods was found to be approximately 1 and 0.5 μm at 2 and 48 h, respectively. We propose that the initially formed spheres had begun to evolve into hexagonal rods at the 2 h time point, and with extended time periods, these rods further interacted with each other or coated the existing spheres. The slower conversion into hexagonal rods with Ni(II) could be due to slower metal ion dissociation from the ligands that allows for the reorganization of the peptide assembly with this metal ion.[53] Through our time point studies, we demonstrate that high-quality 3D hexagonal crystals of GCN4-p2L are accessed within 15−30 min with Zn(II) ions. We further wished to determine the role that metal ion concentration plays on peptide assembly and, therefore, focused on Zn(II) as the metal ion for our next studies.

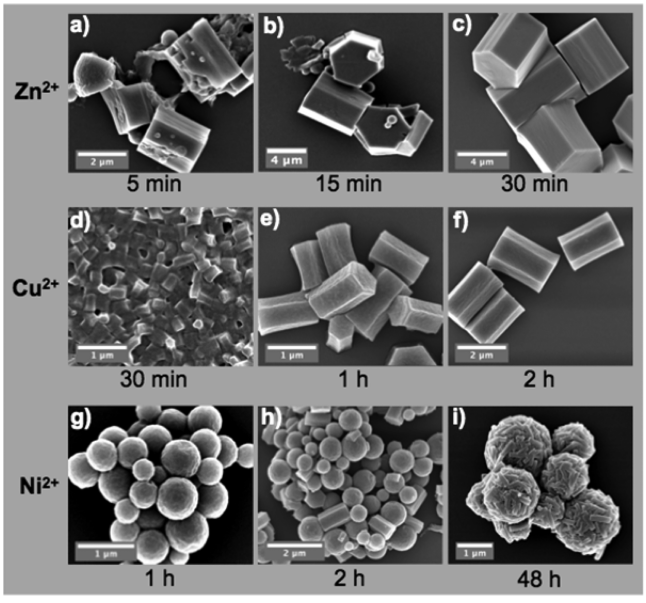

Figure 3. SEM micrographs of the structures obtained from assembly of GCN-p2L (1 mM) with the indicated metal ions (0.4 mM) in 20 mM MOPS buffer at pH 7.1 at the indicated time periods.

Assembly as a Function of Metal Ions. Since our design is based on metal-directed peptide assembly, we investigated the role of Zn(II) ions on the formation of the hexagonal peptide crystals. Incubation of the GCN4-p2L peptide (1.0 mM) without metal ions in MOPS buffer (20 mM, pH 7.1) for 30 min, for instance, generated a fine precipitate that when imaged with SEM displayed an ill-defined, amorphous structure (Supporting Information, Figure S4). Also, treatment of the fully formed hexagonal crystals from GCN4-p2L and Zn(II) with ethylenediaminetetraacetic acid (EDTA) (10 mM) resulted in an immediate and complete dissolution of the crystals. Dynamic light scattering (DLS) was used to monitor the disassembly; the GCN4-p2L and Zn(II) mixture, as described above, was analyzed by DLS after 30 min and showed a distribution of particles with a mean diameter of 1.0 μm, indicating higher-order assembly (Supporting Information, Figure S5). The EDTA-treated sample after about 1 min, however, demonstrated a significant reduction in the mean diameter to ∼5 nm, a value that corresponds roughly to the length of an individual coiled coil. These data demonstrate the importance of metal ions on the formation and integrity of the 3D peptide crystals.

We also investigated metal ion concentration as a factor in the growth of GCN4-p2L crystals. The peptide was treated with 0.1 and 1.0 equiv of Zn(II) to complement the 0.4 equiv data above. At the lower concentration of metal ion, GCN4-p2L yielded hexagonal discs that had a face size similar to that of the crystals shown above (Figure 3c), but the length of the discs was much smaller (Figure 4a,c). However, when the Zn(II) concentration was increased from 0.4 to 1 mM, the hexagonal crystals that formed were slightly thinner (∼3 μm) and longer (Figure 4b,c). Meanwhile, at metal concentrations of 1.2 mM or greater, no visible precipitate was observed with the GCN4-p2L peptide. At these concentrations, it is likely that the metal-binding ligands are fully satisfied with metal ions, thus preventing hierarchical assembly of the peptide sequence. This study not only reiterates the importance of metal ions in the growth of the hexagonal crystals but also provides a powerful means to tune the size of the hexagonal assemblies by varying the concentration of the metal ions.

DOI: 10.1021/jacs.6b06708
J. Am. Chem. Soc. 2016, 138, 11051−11057

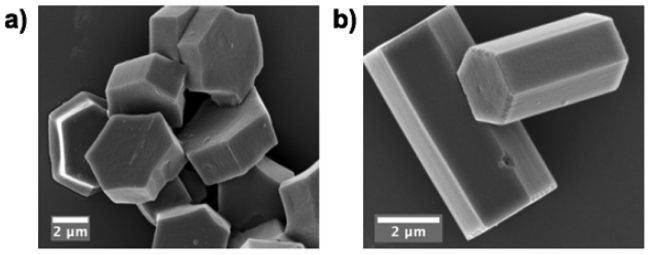

c)

Peptide: Metal	Assembly Length (μm)
1: 0.1	1.9 ± 0.6 (n=25)
1: 0.4	3.8 ± 0.4 (n=50)
1: 1	5.4 ± 0.9 (n=50)

Figure 4. Dependency of the length of the hexagonal assemblies on metal ion concentration. SEM images of structures obtained from assembly of GCN4-p2L (1 mM) with (a) 0.1 mM $ZnCl_2$ and (b) 1 mM $ZnCl_2$ and (c) differences in length of the peptide assemblies at three different peptide to Zn(II) ratios (values in parentheses indicate the number of crystals analyzed).

Structure Determination of Crystals. X-ray diffraction was used to elucidate the structure of the hexagonal crystals obtained from an assembly of a 1.0:0.4 ratio of GCN4-p2L to Zn(II) ions. Data for these crystals were collected at the Advanced Photon Source at Argonne National Laboratory on beamline 23-IDB. Phases were solved by molecular replacement using the GCN4 peptide as a search model (PDB 1ZIM) in Phenix Phaser and the structure refined in Phenix Refine.[54,55] The crystal structure of the peptide assembly was solved to a final resolution of 1.9 Å in the *P*321 space group, reflecting the macroscopic morphology of the crystals (Figure 5). The crystal structure (PDB 5KKV) confirmed the trimeric nature of the coiled coil of GCN4-p2L (Figure 5a,b). The trimers were arranged in a head-to-tail fashion along each metal-directed coiled-coil linear array, and each linear strand was antiparallel to its three neighboring strands (Figure 5b; green and blue indicate linear coiled-coil strands oriented in opposite directions). The interstrand contacts were mediated by a series of hydrogen-bonding interactions from the helix of one coiled coil (blue, Figure 5c) to the helix of a coiled coil in an adjoining strand (green, Figure 5c). These tight junctions led to the tight packing observed in the crystal, with the only lack of strong density occurring at the end of each peptide. The ligands of the peptide and the metal ions were not visible in the crystal structure, although there appears to be room within the crystal lattice for these components (see L in Figure 5a). The lack of electron density may reflect the possibility that these components are intrinsically mobile or not completely occupied, leading to a dispersion in the observed density, meaning these features could not be built into the crystal structure. An X-ray fluorescence scan of the crystals (thoroughly washed with water) produced a fluorescence signal that is characteristic of zinc, consistent with the presence of zinc within the crystals (Supporting Information, Figure S3).

His-Tag-Directed Inclusion of Guests within Crystals. An appealing aspect of the coiled-coil-based crystals is the potential presence of free metal-binding ligands on the surface and perhaps within the crystals. Since the trimeric GCN4-p2L coiled coils are arranged in a head-to-tail fashion, as observed in the crystal structure, we envisioned that the hexagonal faces of the crystals would contain free metal-binding ligands (Figure 6a). These ligands, such as NTA, could be loaded with metal ions and would be available to bind His-tagged cargoes (Figure 6a). Inspired by this concept, we took preformed hexagonal crystals (1:1 peptide/metal ion ratio) and treated them with $NiCl_2$ (1.0 mM) for 1 h, followed by addition of fluorescein-labeled His_6 (Fl-His_6, 0.1 mM) for 3 h.[56] The resulting crystals were washed and visualized using fluorescent confocal

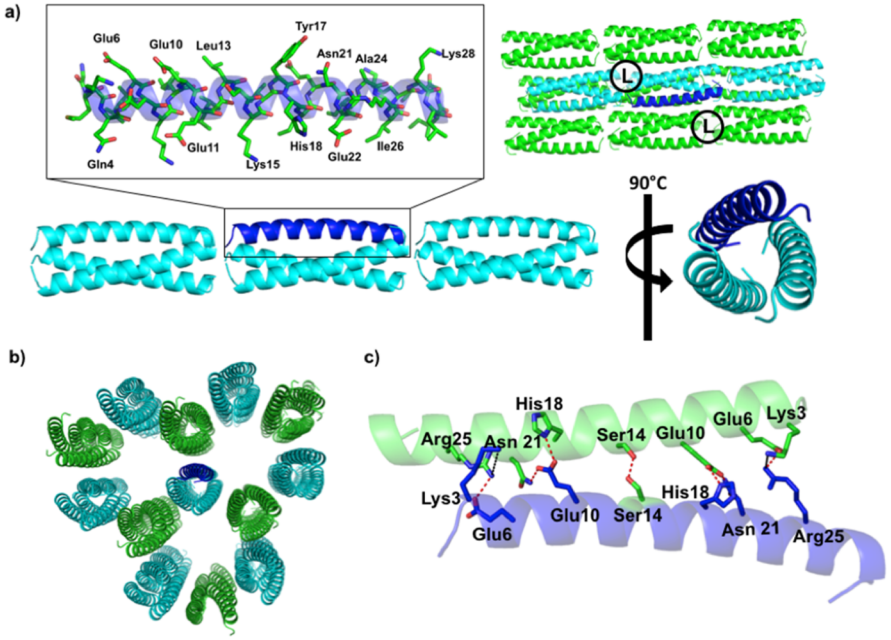

Figure 5. Hexagonal crystal pattern obtained at a resolution of 1.9 Å. (a) Head-to-tail arrangement of the GCN4-p2L peptide in the hexagonal crystal. (b) Top-down view of the arrangement of GCN4-p2L trimers in the crystal lattice: blue coiled coils have the N-termini pointing toward the viewer; green coiled coils have the C-termini toward the viewer. (c) Interactions at the interface of neighboring coiled-coil trimers in the hexagonal crystal.

DOI: 10.1021/jacs.6b06708
J. Am. Chem. Soc. 2016, 138, 11051−11057

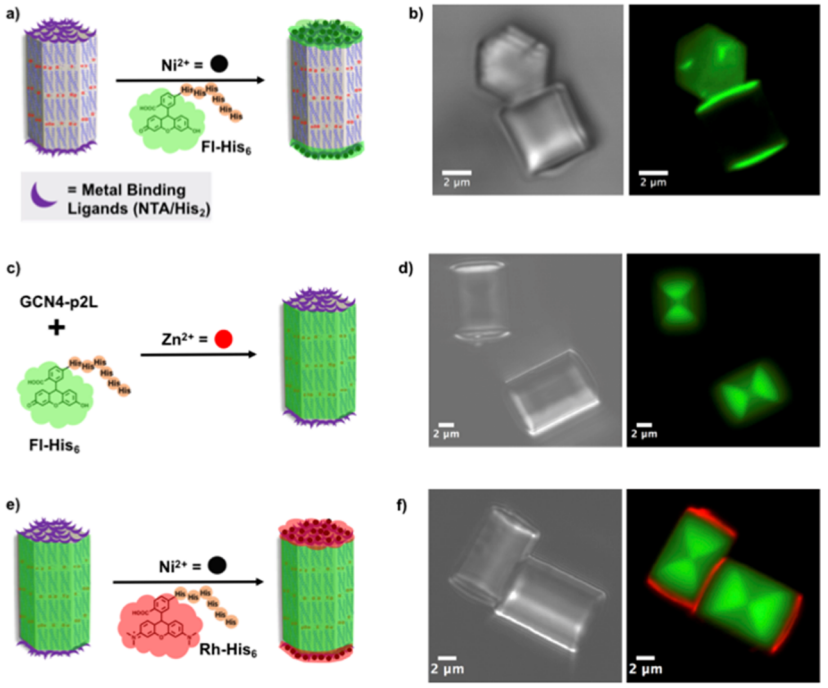

Figure 6. Schematic representations for directing His-tagged fluorophore guests to the Zn(II)/GCN4-p2L crystals: (a) on the surface after crystal formation, (c) within the crystal during formation, or (e) at both the surface and within crystals. Bright-field (left) and confocal (right) microscopy images of (b) hexagonal crystals treated with Fl-His_6 (0.1 mM), (d) Fl-His_6 added during the formation of the crystals, and (f) crystals assembled in the presence of Fl-His_6 (0.1 mM) followed by treatment with Rh-His_6 (0.1 mM) after crystallization.

microscopy. Green fluorescence was observed with all crystals, but the fluorescence was located only at the hexagonal (P3) faces of the crystal (Figure 6b). We found that free fluorescein did not associate with the crystals (Supporting Information, Figure S6b), indicating the importance of the His-tag in directing fluorescein to this crystal face.

As the coiled-coil crystals grew, we investigated if it is also possible to include guests within the core of the crystals in a His-tag-dependent fashion (Figure 6c). Therefore, Fl-His_6 (0.1 mM) was added to the GCN4-p2L peptide solution (1 mM) followed by Zn(II) (1.0 mM) addition. An immediate precipitate formed that was collected after 1 h, thoroughly washed, and visualized by fluorescence confocal microscopy (Figure 6d). Again, all of the crystals now fluoresced green, but the fluorescence was localized to two sections of the crystals, forming an "hourglass" pattern. This pattern originated at the center of the crystals and projected out toward the P3 crystalline faces. A similar pattern was reported for many organic dyes that stain inorganic salts[57] and also for proteins as inclusions within crystals of organic hosts, such as phthalic acid.[58] Generally, the hourglass pattern is observed when the guest has an affinity for two symmetry-related faces on opposing sides of a growing crystal. In our case, the His-tag can bind to the growing P3 face where the ligands are present, and as those faces naturally increase in area as the crystal grows, so do the fluorescent subvolumes associated with these faces (Figure 6d). On the other hand, when fluorescein lacking the His-tag was added to GCN4-p2L, followed by addition of Zn(II), deformed crystals were obtained that mostly were not stained with fluorescein. When fluorescein was found in the crystal, it was in a seemingly random manner toward the center (Supporting Information, Figure S6a). These data demonstrate the essential nature of the His-tag for directing the inclusion of the fluorophore to specific regions of the crystal.

The two strategies for directing guests to the coiled-coil crystals were combined: Fl-His_6 was added to the growing crystal solution as described above, and a rhodamine-labeled His_6 (Rh-His_6) was added after the crystals were formed, also as described above (Figure 6e). Green fluorescence was again observed in an hourglass pattern within the crystals, whereas red fluorescence was found at the hexagonal P3 faces of the crystals (Figure 6f). Overall these His-tagged-directed experiments have demonstrated the facile and distinct incorporation of fluorophore guests on the surface and within the crystals and have provided insights into the mechanism of the metal-promoted crystallization of the GCN4-p2L coiled coils.

■ CONCLUSION

In summary, a metal-mediated head-to-tail assembly strategy was successfully engineered into a coiled-coil trimeric peptide, GCN4-p2L, to form hexagonal 3D crystals in the presence of divalent metal ions. These 3D peptide crystals were easily accessible within 30 min, and their morphology could be controlled by varying the metal ion/peptide ratio, resulting in hexagonal discs to rods. Diffraction studies confirmed the trimeric nature of the peptide construct and elucidated the head-to-tail arrangement of the coiled-coil linear strands and their hexagonal, antiparallel packing within the crystal. Unsatisfied ligands at the hexagonal ends of the crystals were harnessed as a powerful means to direct His-tagged fluorophores to the faces of the crystals, whereas the addition of the His-tagged guest to the crystal-growing solution resulted in the specific incorporation of the guest within two sectors of the crystal, resulting in an hourglass pattern. Both His-tagged strategies were employed to direct guests to contiguous locations within the crystals. This crystal design provides a facile means to obtain 3D peptide crystals on demand and

DOI: 10.1021/jacs.6b06708
J. Am. Chem. Soc. 2016, 138, 11051−11057

incorporate His-tag-based cargoes, thereby enhancing the crystals for potential use as delivery agents, probes, and sensors.

METHODS

Crystal Formation. The GCN4-p2L peptide in 20 mM MOPS buffer (pH 7.1) was treated with the specified metal ion ($ZnCl_2$, $CoCl_2$, $CuCl_2$, and $NiCl_2$) in distilled water at room temperature to provide a final peptide concentration of 1.0 mM and final metal ion concentrations of 0.1, 0.4, or 1.0 mM. At the indicated time, the mixtures were centrifuged at 10 000*g* for 3 min. The assemblies were washed three times with distilled water and resuspended in distilled water prior to analysis by SEM and X-ray diffraction.

His-Tagged Fluorophore Addition−Postcrystal Formation. Hexagonal crystals of the GCN4-p2L peptide (1 mM) and $ZnCl_2$ (1 mM) were prepared as described above for 1 h. The precipitate that formed was washed once with distilled water and treated with $NiCl_2$ (1 mM) for 1 h. The samples were washed again with distilled water, followed by incubation with Fl-His_6 (0.1 mM) for 3 h. The resulting samples were washed three times with distilled water and resuspended in distilled water prior to analysis by confocal microscopy. A droplet of each sample was placed on a coverslip and visualized under an inverted 60× oil objective of a Nikon AIR MP confocal microscope. Fluorescein was excited using a 488 nm excitation laser.

His-Tagged Fluorophore Addition−Precrystal Formation. Hexagonal crystals of the GCN4-p2L peptide (1 mM) and $ZnCl_2$ (1 mM) were prepared as described above but in the presence of Fl-His_6 (0.1 mM) for 1 h. The crystals were washed three times with distilled water and resuspended in distilled water. For the dual labeling, these crystals were treated with $NiCl_2$ (1 mM) for 2 h, washed once with distilled water, followed by addition of Rh-His_6 (0.1 mM) for 3 h. The crystals were washed three times with distilled water and analyzed by confocal microscopy as described above. Fluorescein and rhodamine were excited using 488 and 555 nm excitation lasers, respectively.

ASSOCIATED CONTENT

Supporting Information

The Supporting Information is available free of charge on the ACS Publications website at DOI: 10.1021/jacs.6b06708.

Additional experimental procedures and characterization of peptide including analytical HPLC trace and CD spectrum; experimental data for assemblies such as DLS, X-ray fluorescence scan, X-ray crystallography details, and confocal microscopy images (PDF)

AUTHOR INFORMATION

Corresponding Author

*chml@purdue.edu

Notes

The authors declare no competing financial interest.

ACKNOWLEDGMENTS

This work was supported by the National Science Foundation through Grant CHE1609406. We thank Rashmi Shrestha for assistance with the crystallographic data and Bart Kahr for helpful discussions.

REFERENCES

(1) Margolin, A. L.; Navia, M. A. *Angew. Chem., Int. Ed.* **2001**, *40*, 2204.
(2) Pechenov, S.; Shenoy, B.; Yang, M. X.; Basu, S. K.; Margolin, A. L. *J. Controlled Release* **2004**, *96*, 149.
(3) Basu, S. K.; Govardhan, C. P.; Jung, C. W.; Margolin, A. L. *Expert Opin. Biol. Ther.* **2004**, *4*, 301.
(4) Ueno, T. *Chem. - Eur. J.* **2013**, *19*, 9096.
(5) Lanci, C. J.; MacDermaid, C. M.; Kang, S. G.; Acharya, R.; North, B.; Yang, X.; Qiu, X. J.; DeGrado, W. F.; Saven, J. G. *Proc. Natl. Acad. Sci. U. S. A.* **2012**, *109*, 7304.
(6) Ogihara, N. L.; Weiss, M. S.; Degrado, W. F.; Eisenberg, D. *Protein Sci.* **1997**, *6*, 80.
(7) Brodin, J. D.; Ambroggio, X. I.; Tang, C.; Parent, K. N.; Baker, T. S.; Tezcan, F. A. *Nat. Chem.* **2012**, *4*, 375.
(8) King, N. P.; Bale, J. B.; Sheffler, W.; McNamara, D. E.; Gonen, S.; Gonen, T.; Yeates, T. O.; Baker, D. *Nature* **2014**, *510*, 103.
(9) Sakai, F.; Yang, G.; Weiss, M. S.; Liu, Y.; Chen, G.; Jiang, M. *Nat. Commun.* **2014**, *5*, 4634.
(10) Sontz, P. A.; Bailey, J. B.; Ahn, S.; Tezcan, F. A. *J. Am. Chem. Soc.* **2015**, *137*, 11598.
(11) Potekhin, S. A.; Melnik, T. N.; Popov, V.; Lanina, N. F.; Vazina, A. A.; Rigler, P.; Verdini, A. S.; Corradin, G.; Kajava, A. V. *Chem. Biol.* **2001**, *8*, 1025.
(12) Ogihara, N. L.; Ghirlanda, G.; Bryson, J. W.; Gingery, M.; DeGrado, W. F.; Eisenberg, D. *Proc. Natl. Acad. Sci. U. S. A.* **2001**, *98*, 1404.
(13) Zhou, M.; Bentley, D.; Ghosh, I. *J. Am. Chem. Soc.* **2004**, *126*, 734.
(14) Lomander, A.; Hwang, W.; Zhang, S. *Nano Lett.* **2005**, *5*, 1255.
(15) Zimenkov, Y.; Dublin, S. N.; Ni, R.; Tu, R. S.; Breedveld, V.; Apkarian, R. P.; Conticello, V. P. *J. Am. Chem. Soc.* **2006**, *128*, 6770.
(16) Ryadnov, M. G. *Angew. Chem., Int. Ed.* **2007**, *46*, 969.
(17) Ulijn, R. V.; Smith, A. M. *Chem. Soc. Rev.* **2008**, *37*, 664.
(18) Robson Marsden, H.; Kros, A. *Angew. Chem., Int. Ed.* **2010**, *49*, 2988.
(19) Fletcher, J. M.; Harniman, R. L.; Barnes, F. R.; Boyle, A. L.; Collins, A.; Mantell, J.; Sharp, T. H.; Antognozzi, M.; Booth, P. J.; Linden, N.; Miles, M. J.; Sessions, R. B.; Verkade, P.; Woolfson, D. N. *Science* **2013**, *340*, 595.
(20) Xu, C.; Liu, R.; Mehta, A. K.; Guerrero-Ferreira, R. C.; Wright, E. R.; Dunin-Horkawicz, S.; Morris, K.; Serpell, L. C.; Zuo, X.; Wall, J. S.; Conticello, V. P. *J. Am. Chem. Soc.* **2013**, *135*, 15565.
(21) Gradisar, H.; Bozic, S.; Doles, T.; Vengust, D.; Hafner-Bratkovic, I.; Mertelj, A.; Webb, B.; Sali, A.; Klavzar, S.; Jerala, R. *Nat. Chem. Biol.* **2013**, *9*, 362.
(22) Ramakers, B. E.; van Hest, J. C.; Lowik, D. W. *Chem. Soc. Rev.* **2014**, *43*, 2743.
(23) Hume, J.; Sun, J.; Jacquet, R.; Renfrew, P. D.; Martin, J. A.; Bonneau, R.; Gilchrist, M. L.; Montclare, J. K. *Biomacromolecules* **2014**, *15*, 3503.
(24) Egelman, E. H.; Xu, C.; DiMaio, F.; Magnotti, E.; Modlin, C.; Yu, X.; Wright, E.; Baker, D.; Conticello, V. P. *Structure* **2015**, *23*, 280.
(25) Burgess, N. C.; Sharp, T. H.; Thomas, F.; Wood, C. W.; Thomson, A. R.; Zaccai, N. R.; Brady, R. L.; Serpell, L. C.; Woolfson, D. N. *J. Am. Chem. Soc.* **2015**, *137*, 10554.
(26) Sharp, T. H.; Bruning, M.; Mantell, J.; Sessions, R. B.; Thomson, A. R.; Zaccai, N. R.; Brady, R. L.; Verkade, P.; Woolfson, D. N. *Proc. Natl. Acad. Sci. U. S. A.* **2012**, *109*, 13266.
(27) Ringler, P.; Schulz, G. E. *Science* **2003**, *302*, 106.
(28) Dexter, A. F.; Malcolm, A. S.; Middelberg, A. P. *Nat. Mater.* **2006**, *5*, 502.
(29) Stendahl, J. C.; Rao, M. S.; Guler, M. O.; Stupp, S. I. *Adv. Funct. Mater.* **2006**, *16*, 499.
(30) Burazerovic, S.; Gradinaru, J.; Pierron, J.; Ward, T. R. *Angew. Chem., Int. Ed.* **2007**, *46*, 5510.
(31) Tsurkan, M. V.; Ogawa, M. Y. *Biomacromolecules* **2007**, *8*, 3908.
(32) Dublin, S. N.; Conticello, V. P. *J. Am. Chem. Soc.* **2008**, *130*, 49.
(33) Przybyla, D. E.; Chmielewski, J. *J. Am. Chem. Soc.* **2008**, *130*, 12610.
(34) Pires, M. M.; Przybyla, D. E.; Chmielewski, J. *Angew. Chem., Int. Ed.* **2009**, *48*, 7813.
(35) Pires, M. M.; Chmielewski, J. *J. Am. Chem. Soc.* **2009**, *131*, 2706.
(36) Zaytsev, D. V.; Xie, F.; Mukherjee, M.; Bludin, A.; Demeler, B.; Breece, R. M.; Tierney, D. L.; Ogawa, M. Y. *Biomacromolecules* **2010**, *11*, 2602.
(37) Ni, T. W.; Tezcan, F. A. *Angew. Chem., Int. Ed.* **2010**, *49*, 7014.

DOI: 10.1021/jacs.6b06708
J. Am. Chem. Soc. 2016, 138, 11051−11057

(38) Bogdan, N. D.; Matache, M.; Roiban, G. D.; Dobrota, C.; Meier, V. M.; Funeriu, D. P. *Biomacromolecules* **2011**, *12*, 3400.
(39) Micklitsch, C. M.; Knerr, P. J.; Branco, M. C.; Nagarkar, R.; Pochan, D. J.; Schneider, J. P. *Angew. Chem., Int. Ed.* **2011**, *50*, 1577.
(40) Knerr, P. J.; Branco, M. C.; Nagarkar, R.; Pochan, D. J.; Schneider, J. P. *J. Mater. Chem.* **2012**, *22*, 1352.
(41) Anzini, P.; Xu, C.; Hughes, S.; Magnotti, E.; Jiang, T.; Hemmingsen, L.; Demeler, B.; Conticello, V. P. *J. Am. Chem. Soc.* **2013**, *135*, 10278.
(42) Brodin, J. D.; Smith, S. J.; Carr, J. R.; Tezcan, F. A. *J. Am. Chem. Soc.* **2015**, *137*, 10468.
(43) Zou, R.; Wang, Q.; Wu, J.; Wu, J.; Schmuck, C.; Tian, H. *Chem. Soc. Rev.* **2015**, *44*, 5200.
(44) Gunasekar, S. K.; Anjia, L.; Matsui, H.; Montclare, J. K. *Adv. Funct. Mater.* **2012**, *22*, 2154.
(45) Harbury, P. B.; Zhang, T.; Kim, P. S.; Alber, T. *Science* **1993**, *262*, 1401.
(46) Shoemaker, K. R.; Kim, P. S.; York, E. J.; Stewart, J. M.; Baldwin, R. L. *Nature* **1987**, *326*, 563.
(47) Burkhard, P.; Ivaninskii, S.; Lustig, A. *J. Mol. Biol.* **2002**, *318*, 901.
(48) Heeres, J. T.; Kim, S. H.; Leslie, B. J.; Lidstone, E. A.; Cunningham, B. T.; Hergenrother, P. J. *J. Am. Chem. Soc.* **2009**, *131*, 18202.
(49) Holzwarth, G.; Doty, P. *J. Am. Chem. Soc.* **1965**, *87*, 218.
(50) Greenfield, N. J. *Nat. Protoc.* **2006**, *1*, 2876.
(51) Lau, S. Y.; Taneja, A. K.; Hodges, R. S. *J. Biol. Chem.* **1984**, *259*, 13253.
(52) Hart, B. R.; Shea, K. J. *Macromolecules* **2002**, *35*, 6192.
(53) Grindy, S. C.; Learsch, R.; Mozhdehi, D.; Cheng, J.; Barrett, D. G.; Guan, Z.; Messersmith, P. B.; Holten-Andersen, N. *Nat. Mater.* **2015**, *14*, 1210.
(54) Gonzalez, L., Jr.; Woolfson, D. N.; Alber, T. *Nat. Struct. Biol.* **1996**, *3*, 1011.
(55) Adams, P. D.; Afonine, P. V.; Bunkoczi, G.; Chen, V. B.; Davis, I. W.; Echols, N.; Headd, J. J.; Hung, L. W.; Kapral, G. J.; Grosse-Kunstleve, R. W.; McCoy, A. J.; Moriarty, N. W.; Oeffner, R.; Read, R. J.; Richardson, D. C.; Richardson, J. S.; Terwilliger, T. C.; Zwart, P. H. *Acta Crystallogr., Sect. D: Biol. Crystallogr.* **2010**, *66*, 213.
(56) Pires, M.; Ernenwein, D.; Chmielewski, J. *Biomacromolecules* **2011**, *12*, 2429.
(57) Kahr, B.; Gurney, R. W. *Chem. Rev.* **2001**, *101*, 893.
(58) Chmielewski, J.; Lewis, J. J.; Lovell, S.; Zutshi, R.; Savickas, P.; Mitchell, C. A.; Subramony, J. A.; Kahr, B. *J. Am. Chem. Soc.* **1997**, *119*, 10565.

DOI: 10.1021/jacs.6b06708
J. Am. Chem. Soc. 2016, 138, 11051−11057